We are IntechOpen, the world's leading publisher of Open Access books Built by scientists, for scientists

4,800
Open access books available

122,000
International authors and editors

135M
Downloads

Our authors are among the

154
Countries delivered to

TOP 1%
most cited scientists

12.2%
Contributors from top 500 universities

CLARIVATE ANALYTICS BOOK CITATION INDEX INDEXED

WEB OF SCIENCE™

Selection of our books indexed in the Book Citation Index in Web of Science™ Core Collection (BKCI)

Interested in publishing with us?
Contact book.department@intechopen.com

Numbers displayed above are based on latest data collected.
For more information visit www.intechopen.com

4

Hysteresis behaviour and modeling of SMA actuators

Hongyan Luo[1,2], Yanjian Liao[1], Eric Abel[2], Zhigang Wang[2] and Xia Liu[1]
[1]*Chongqing University*
P.R. China
[2]*University of Dundee*
UK

1. Introduction

In recent years, the use of shape memory alloy (SMA) as a key component in diverse actuation applications has attracted more interests, especially in the field of mechatronics and medical instruments (Wolfe et al, 2005; Wong et al, 2007; Gupta et al, 2009, Okamura et al, 2009, De Sars et al, 2010). The positive features of good reliability, high energy density, design simplicity, compactness in configuration and quiet operation, point to SMA being a promising candidate for actuator. However, great difficulties are always encountered in the precise control of the systems incorporating them, due mainly to the nonlinearities of the complex hysteresis associated with the shape memory effect. These nonlinearities must be considered and dealt with properly, since they may excite unwanted dynamics that lead in the best scenario to a deteriorated system performance and in the worst scenario to an unstable dynamic system.

One effective method to compensate for such hysteresis nonlinearities is to involve a model in the control scheme that is able to describe the complex nonlinear behaviour of SMA actuators and accordingly give reliable predictions of the system response. In this case, the crucial part of the development lies in accurate modelling of the actual hysteresis nonlinearity. From the viewpoint of control, such a hysteresis model should characterize the nonlinearities with sufficient accuracy, be amenable to a compensator design for actuator linearization and be well-suited for real-time applications. Therefore, the usual constitutive models (Bhattacharyya & Lagoudas, 1997; Matsuzaki & Naito, 2004; Popov & Lagoudas, 2007; Wang & Dai, 2010), derived from thermodynamical or micromechanical principles, are immediately discarded for this purpose, owing to the mathematical complexity involved and non-availability of the microstructural material parameters.

This chapter starts with the description of the hysteresis behaviour of SMA actuators. Following the analysis of its hysteresis characteristics, a phenomenological model based on the theory of hysteresis operator, referred to as MKP model, is proposed and its inverse model is deduced with the aim to provide a more appropriate choice for the modelling of

the hysteretic system incorporating SMA actuator for control applications. The computer simulations are also presented to verify this model.

2. Hysteresis characteristics of SMA actuators

The hysteresis behaviour of SMA actuators associated with shape memory effect is characterized by the fact that there are multiple possible outputs (i.e. strain or displacement) with respect to a given input (i.e. temperature). At any time, the specific output is determined by the current input and the previous inputs (i.e. input history). This type of relationship between input and output, given the name of hysteresis, is a byproduct of phase transitions that take place in SMA, and is caused by the internal friction generated by the movement of the austenite-martensite interface and by the creation of structural defects within the alloy structure (Wayman & Duerig, 1990). This strain-temperature hysteresis is present in all systems incorporating SMA actuators and is an important consideration in their control.

To give a demonstration of such hysteresis behaviour, some sample curves were measured on a NiTi tension spring under a load by alternately heating and cooling it between the temperature lower than its martensite finish temperature (Mf) and the temperature higher than its austenite finish temperature (Af). Fig.1 gives a typical temperature-displacement curve where the points at which the temperature gradient changes its sign, known as return points, are marked by number. The curve shows a major loop enclosing a group of minor loops.

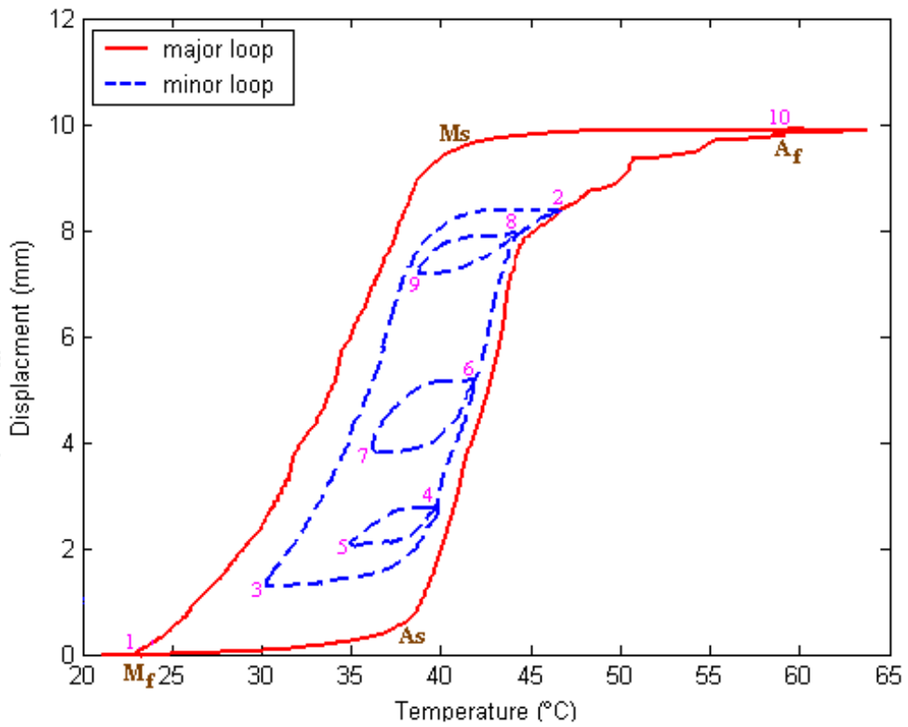

Fig. 1. A typical hysteresis curve of an SMA actuator by the example of a NiTi tension spring

The major loop is the full-scale strain trajectory corresponding to a complete actuation cycle of an SMA actuator, which is achieved by heating and cooling the actuator throughout its overall transformation temperature range defined by Mf (lower limit) and Af (upper limit). The minor loop corresponds to the partial strain excursion within the strain range of the SMA actuator caused by heating and cooling the actuator through part of its transformation temperature range, i.e. the incomplete actuation. Although the specific shape and width of hysteresis loop are related to alloy composition and the fabrication process (Van Humbeeck & Stalmans, 1998), there seems to be general agreement in the literature on the main features of SMA hysteresis response observed experimentally, such as closed loops between two return points, path dependency, self-containment and return point memory (Ŝittner et al, 2000).

Noticeably, for the same SMA actuator, the envelope of its hysteresis curve, i.e. the major loop, does not keep constant, but varies with the applied loading and the amount of strain prior to actuation, as illustrated in Fig. 2. It can be seen that both the increasing mass applied to the SMA actuator and the increasing compressed length (i.e. pre-deformation), cause the major loop of the SMA actuator to expand vertically. Inside the major loop, any minor loop, which is formed by reversing the actuation direction of SMA actuator in the state of mixed martensite and austenite, is mainly determined by the internal microstructure or rather the interaction of co-existing martensite and austenite, depending on the temperature history.

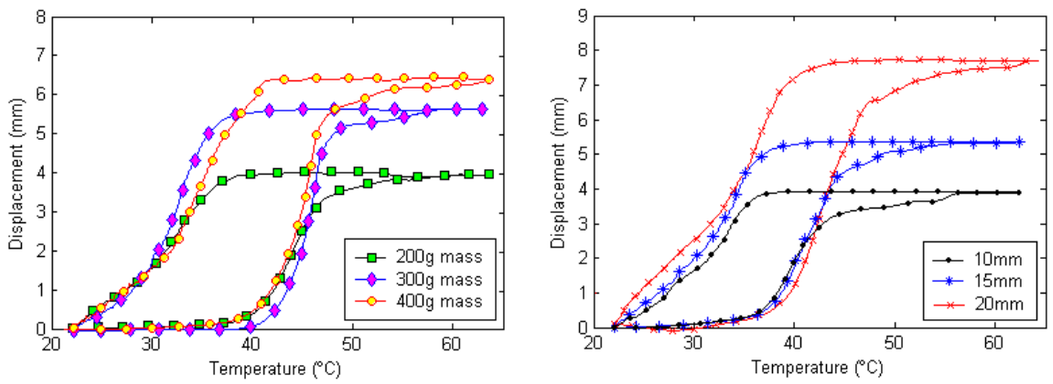

(a) Major loops for different masses (b) Major loops for different pre-deformation

Fig. 2. Influence of applied loading and pre-deformation on hysteresis behaviour of SMA actuators

On one hand, the common characteristics in the hysteresis behaviour allow the possibility of a purely phenomenological model to generally represent the hysteresis response of various SMA actuator based systems, regardless of the type of SMA actuator involved and the underlying physics. On the other hand, the complex hysteresis behaviour, which is influenced by both external and internal factors, makes it a challenge to implement algorithms for the hysteresis modelling in dynamic service environments, since a great deal of parametric uncertainties are involved. In particular, the modelling issue becomes much more complicated in the application of SMA actuators under controlled actuation, where they typically work in partial cycles and thus many minor loops would be encountered rather than a single major loop in the case of on-off applications. Furthermore, for real-time control applications, the complexity of algorithm implementation and computational burden associated with the phenomenological model are especially concerned.

3. MKP hysteresis model

The MKP hysteresis model proposed here is actually a mutation of the classical Preisach model, which is a well-known phenomenological hysteresis model and based on the general theory of hysteresis operators (Krasnoselskii & Pokrovskii, 1989). The rest of this section only covers the main principles of this theory. A more complete description is available elsewhere (Mayergoye, 1991; Krasnoselskii et al, 1994; Webb & Lagoudas, 1998).

3.1 Principle and mathematical formalism

The concept of hysteresis operator modelling was first proposed in 1935 by the physician Preisach as a restricted physical representative for ferromagnetic hysteresis phenomenon, called Preisach model. About thirty years later, its nature in phenomenology was noticed and the mathematical properties were investigated by the mathematicians (Krasnoselskii & Pokrovskii, 1989), who separated this model from its physical meaning and represented it in a purely mathematical form as follows:

$$Y = H[T(t)] = \iint_{(\alpha,\beta)\in S} \mu(\alpha,\beta)\gamma_{\alpha\beta}(T,\xi_{\alpha\beta})d\beta d\alpha \tag{1}$$

Here $T(t)$ is the input (i.e. temperature for SMA actuator), $\hat{\gamma}_{\alpha\beta}$ is an elementary hysteresis operator function that gives the current states of the hysteresis operators in response to the input variation, the variable $\xi_{\alpha\beta}$ represents the previous state of the hysteresis operator, $\mu(\alpha,\beta)$ is the density distribution function, also called Preisach function, to define the weighting values for these operators, which captures characteristics of the specific hysteresis system, and S is the Preisach plane, i.e. the region over which hysteresis occurs, defined by the input region as follows:

$$S = \left\{(\alpha,\beta) : T_{\min} \le \alpha \le \beta, T_{\min} \le \beta \le T_{\max}\right\}$$

The integration takes the past input history into account to determine the current output.
For numerical implementation, a finite-dimensional approximation of equation (1) is deduced as

$$Y = H(T) = \sum_{j=1}^{K}\sum_{i=1}^{j} \gamma_{s_{ij}}(T,\xi_{s_{ij}})\mu_{s_{ij}} \tag{2}$$

by uniformly dividing the Preisach plane into a mesh grid (i.e. the discrete Preisach plane) of $K \times K$ with an interval of $\Delta T = (T_{\max} - T_{\min})/(K-1)$, as shown in Fig.3. Then the number of grid points representing the Preisach plane is given by $N = K \times (K+1)/2$. In the discrete Preisach plane, there exists a hysteresis operator $\gamma_{s_{ij}}(T,\xi_{s_{ij}})$ and a weighting value $\mu_{s_{ij}}$ for each grid point $s_{ij} = (\alpha_i, \beta_j)$, where

$$\alpha_i = T_{\min} + (i-1)\Delta T\ ,\ \beta_j = T_{\min} + (j-1)\Delta T \tag{3}$$

for $j = 1,2,\cdots,K$, $i = 1,2,\cdots,j$. As $K \to \infty$, the discretization becomes finer and finer, approaching the continuous Preisach plane. In the discrete Preisach plane, there exists a hysteresis operator $\gamma_{s_{ij}}(T,\xi_{s_{ij}})$ and a weighting value $\mu_{s_{ij}}$ for each grid point s_{ij} . In other

words, each operator is identified by only one particular grid point, which is uniquely defined by a pair of α and β coordinates.

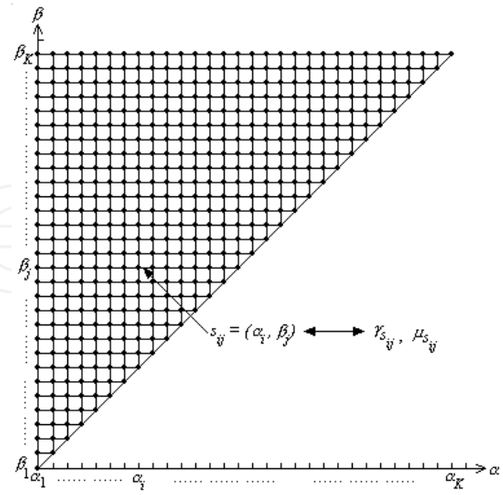

Fig. 3. Discretization of Preisach plane

The numerical approximation (see equation 2) apparently indicates that hysteresis operator modelling can be represented by a straightforward structure, analogous to the parallel connections of a series of qualitatively similar elements, as illustrated by the block diagram in Fig.4.

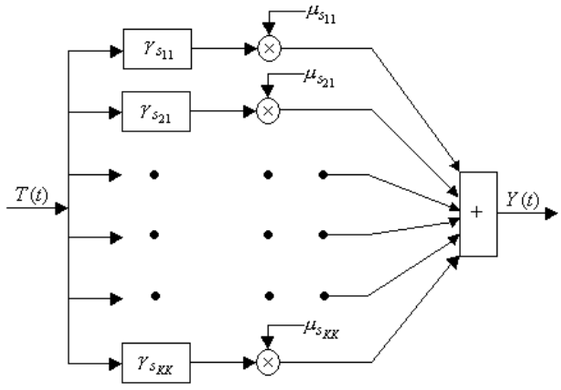

Fig. 4. Block diagram of hysteresis operator theory

Clearly, the above formalism presents a general mathematical tool for hysteresis modelling, which can be adjusted to capture the input-output features of the different hysteresis systems by the appropriate selection of the elementary hysteresis operator and of the density distribution function. This has allowed its applications to been extended from a ferromagnetic material to smart materials such as piezoceramic and SMA (Dickinson et al, 1996; Hughes & Wen, 1997).

3.2 MKP hysteresis operator

The building block of this hysteresis modelling approach is an elementary hysteresis operator, which is non-complicated hysteresis nonlinearity with a simple mathematical

structure characterized by one or more parameters. The different types of elementary hysteresis operators in use account for the differences in the models based on the theory of hysteresis operator. The typical elementary hysteresis operators are relay operator and KP operator, which are used in the classical Preisach model and KP model respectively. The examples of these two types of hysteresis operator and MKP operator for use in MKP model, corresponding to a grid point $s_{ij} = (\alpha_i, \beta_j)$ in the discrete Preisach plane, are given in Fig. 5.

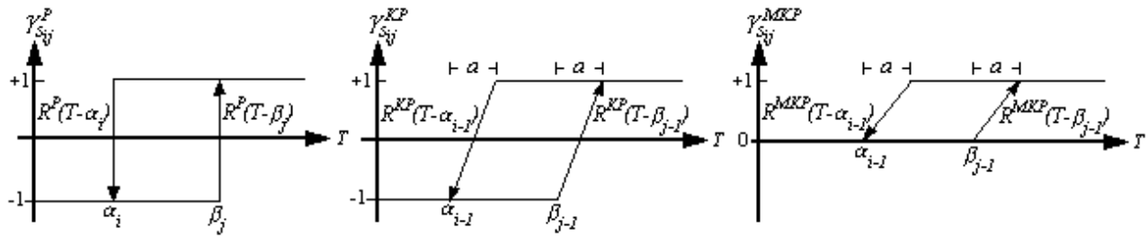

(a) Relay operator (b) KP operator (c) MKP operator

Fig. 5. Three types of elementary hysteresis operator

The relay operator is the simplest operator with only two output states, and characterized by a step transition between –1 and +1. The KP operator is a continuous version of relay operator, developed by Krasnoselskii and Pokrovskii (Krasnoselskii & Pokrovskii 1994), which can exist at any value in the closed interval of $[-1,+1]$ rather than at the two extreme ends. Due to this continuity, the KP model can describe a real hysteresis I/O relationship more closely than can the Preisach model. It is useful to point out that the selection of –1 and +1 as the extreme state values for both the relay operator and the KP operator arises from the initially physical motivation of the hysteresis operator theory that each elementary hysteresis operator represents one magnetic dipole changing between the negative magnetic polarity and the positive magnetic polarity (Hughes & Wen, 1997). This boundary condition is not compulsory for the definition of elementary hysteresis operator in terms of the mathematical meaning of this modelling theory, which need not be conformed to especially when it is used for modelling other materials. Therefore, the MKP operator is given here by simply halving the output range of the KP operator to $[0,+1]$.

Referring to Fig.5(c), the ridge function of a MKP operator is defined by

$$r(x) = \begin{cases} 0 & x < 0 \\ \dfrac{x}{a} & 0 \le x \le a \\ 1 & x > a \end{cases} \tag{4}$$

where $x = T - \alpha_{i-1}$ for the left bounding curve, $x = T - \beta_{j-1}$ for the right bounding curve. The rise interval of input a is set as ΔT, over which the operator changes value between 0 and 1. The mathematical representation, which describes the action of a MKP operator is given by

$$\gamma_{s_{ij}}(T,\xi_{s_{ij}}) = \begin{cases} \max\left\langle \xi_{s_{ij}}, r(T-\beta_{j-1}) \right\rangle & \dot{T} > 0 \\ \min\left\langle \xi_{s_{ij}}, r(T-\alpha_{i-1}) \right\rangle & \dot{T} < 0 \\ \xi_{s_{ij}} & \dot{T} = 0 \end{cases} \tag{5}$$

where $\dot{T}$ represents the direction of temperature change and the memory term (i.e. $\xi_{s_{ij}}$) for a specific MKP operator is always updated by the instantaneous value of $\gamma_{s_{ij}}$.

3.3 Advantages of MKP model

Fig.6(a-d) shows how the Preisach plane evolves and how MKP operators respond to input changes. When input is lower than $T_{\min}$, all the MKP operators are 'off' at the minimum output state. As input increases, a horizontal line slides along the positive β direction with the operators just above it as a horizontal boundary, below which all the operators are switched to the maximum output state. Following the decreasing input, a vertical line sweeps in the negative α direction with the operators right next to this line as a vertical boundary, right to which all the operators are changed back to minimum output state. For a sequence of input alternating between $T_{\min}$ and $T_{\max}$, a staircase interface line (i.e. boundary) is created. From the viewpoint of a geometrical interpretation, the Praisach plane at each time instant is divided into two parts: $S_{\max}$ where the operators are at the maximum output state (dark grey), $S_{\min}$ where the operators are at the minimum output state (light grey), by a boundary (S_{bon}) where the operators are at the intermediate state. By comparing the evolution of Preisach plane regarding MKP model, Preisach model and KP model, the advantages of MKP model over the other two can be revealed. Firstly, owing to the minimum output state of 0, the MKP operators in the area $S_{\min}$ make no contribution to the output of the MKP model and need not be taken into account. As a result, the MKP model is more efficient in calculation than KP model and Preisach model, which makes it more suitable for real-time control applications. This advantage is more outstanding, when the discretization of Preisach plane becomes finer and the number of parameters is vast. Secondly, for a SMA based system, its output is usually measured in terms of displacement relative to its initial position, so that its output range is defined as $[0, Y_{\max}]$. Evidently, this is well matched by the output range of MKP model, i.e. $[0, H(T_{\max})]$. These features allow MKP model to be a more appropriate choice for the modelling of the hysteretic system incorporating SMA actuator.

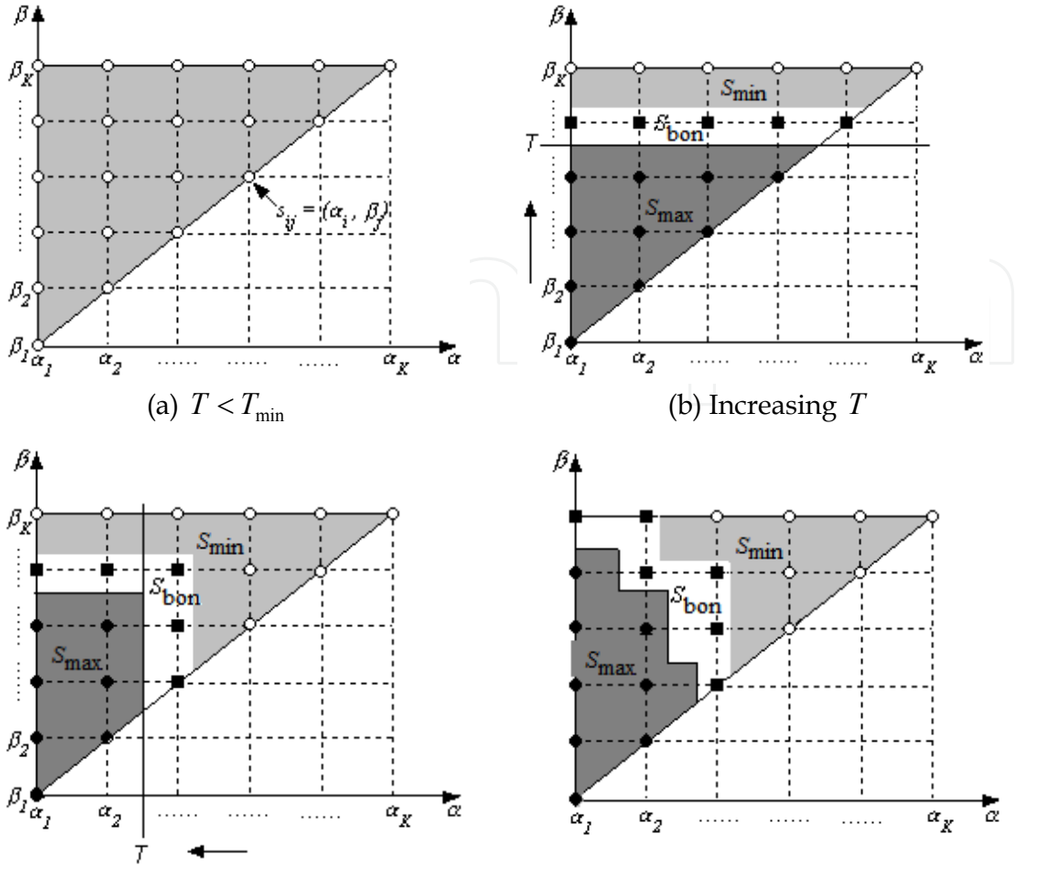

(a) $T < T_{\min}$ (b) Increasing T

(c) Decreasing T (d) Alternating T between $T_{\min}$ and $T_{\max}$

Fig. 6. Evolution of Preisach plane

(o: 0 valued operator; ■: (0,1) valued operator; •: 1 valued operator)

4. Inverse MKP hysteresis model

In fact, the MKP model that gives an input-output mapping cannot directly serve the control applications, since the hysteresis system is often required to follow a reference trajectory, a situation that the desired output is always known, while the corresponding input is unknown. Therefore, it is exactly the inverse MKP model with the capability to predict an input corresponding to a desired output can act as a compensator in control schemes to tackle the hysteresis nonlinearity.

The inverse MKP hysteresis model, represented by $H^{-1}(Y)$, can be easily formulated, after understanding how MKP operators respond to input changes. Let the current input be $T_c \in (\beta_{p-1}, \beta_p]$ and the corresponding output be Y_c. Consider the case of increasing output first.

If the next target output is $Y_d > Y_c$, the goal is to determine T_d so that $Y_d = H(T_d)$. According to the monotonicity, $Y_d > Y_c$ indicates $T_d > T_c$. Therefore, the MKP operators should be

evolved along the positive β axis. By starting the direct calculation of the forward MKP hysteresis model from $T = \beta_p$ in increment of ΔT until $H(\beta_m) \geq Y_d$, it can be determined that $T_d \in (\beta_{m-1}, \beta_m]$. Recalling the previously introduced geometrical interpretation of MKP model (see section 3.3), the final link of the interface to be created by T_d in the Preisach plane is a horizontal one and appears on the row m. Then only the output states of the MKP operators locating on this row may be related to T_d, while all the MKP operators locating on the rows lower than m will have the maximum output states of +1 and those locating on the rows higher than m will keep the previous output states. Referring to the definition of MKP operator function (equation (4),(5)), this can be expressed analytically as

$$\begin{cases} 1 & \text{for } j = 1,2,\cdots,m-1 \text{ and } i = 1,2,\cdots,j \\ \gamma_{s_{ij}}(T_d, \xi_{s_{ij}}) = \xi_{s_{ij}} & \text{for } j = m+1, m+2,\cdots,K \text{ and } i = 1,2,\cdots,j \\ \max\left\langle \xi_{s_{ij}}, \dfrac{T_d - \beta_{m-1}}{\Delta T} \right\rangle & \text{for } j = m \text{ and } i = 1,2,\cdots,m \end{cases} \tag{6}$$

Then the calculation of Y_d can be expressed as

$$Y_d = \sum_{j=1}^{m-1}\sum_{i=1}^{j} \mu_{s_{ij}} + \sum_{j=m+1}^{K}\sum_{i=1}^{j} \xi_{s_{ij}} \mu_{s_{ij}} + \sum_{i=1}^{m} \gamma_{s_{im}}(T_d, \xi_{im}) \mu_{s_{im}} \tag{7}$$

Clearly, the output states of the operators on the row m will change differently, depending on their previous output states and the exact value of T_d. For the most general discussion, assume the past input history causes a staircase line between β_{m-1} and β_m, and the operators on the row m have the previous output states as shown in Fig. 7.

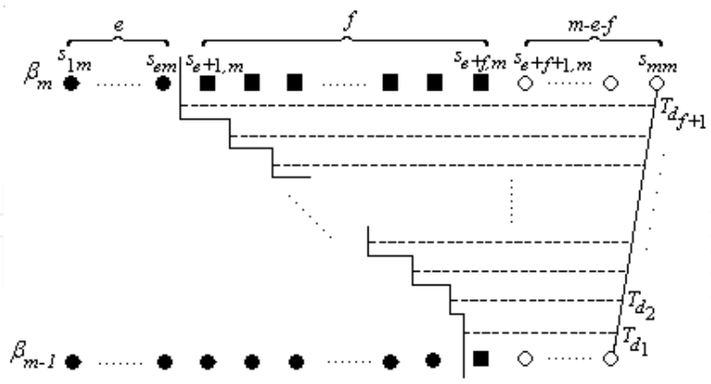

Fig. 7. Example of inverse MKP model for the increasing desired output

(o: 0 valued operator; ■: (0,1) valued operator; •: 1 valued operator)

Then the following results can be obtained:
For $i = 1,2,\cdots,e$, since $\xi_{im} = 1$, there exists

$$\gamma_{s_{im}}(T_d, \xi_{s_{im}}) = \max\left\langle 1, \frac{T_d - \beta_{m-1}}{\Delta T} \right\rangle = 1$$

For $i = e+f+1, e+f+2, \cdots, m$, since $\xi_{im} = 0$, there exists

$$\gamma_{s_{im}}(T_d, \xi_{s_{im}}) = \max\left\langle 0, \frac{T_d - \beta_{m-1}}{\Delta T} \right\rangle = \frac{T_d - \beta_{m-1}}{\Delta T}$$

For $i = e+1, e+2, \cdots, e+f$, since $0 < \xi_{im} < 1$, there are $f+1$ possible situations, namely,

i) $\gamma_{s_{im}}(T_d, \xi_{s_{im}}) = \xi_{s_{im}}$, for $i = e+1, e+2, \cdots, e+f$

ii) $$\gamma_{s_{im}}(T_d, \xi_{s_{im}}) = \begin{cases} \xi_{s_{im}} & \text{for } i = e+1, e+2, \cdots, e+f-1 \\ \dfrac{T_d - \beta_{m-1}}{\Delta T} & \text{for } i = e+f \end{cases}$$

iii) $$\gamma_{s_{im}}(T_d, \xi_{s_{im}}) = \begin{cases} \xi_{s_{im}} & \text{for } i = e+1, e+2, \cdots, e+f-2 \\ \dfrac{T_d - \beta_{m-1}}{\Delta T} & \text{for } i = e+f-1, e+f \end{cases}$$

…

$f+1)$ $\gamma_{s_{im}}(T_d, \xi_{s_{im}}) = \dfrac{T_d - \beta_{m-1}}{\Delta T}$, for $i = e+1, e+2, \cdots, e+f$

This indicates that there are $f+1$ possible solutions for T_d. Let n be the number of the operators that are switched from the previous intermediate output states to the new ones in each case, i.e. $n = 0,1,\cdots,f$. The equation (7) can be rewritten as

$$Y_d = \sum_{j=1}^{m-1}\sum_{i=1}^{j}\mu_{s_{ij}} + \sum_{j=m+1}^{K}\sum_{i=1}^{j}\xi_{s_{ij}}\mu_{s_{ij}} + \sum_{i=1}^{e}\mu_{s_{im}} + \sum_{i=e+1}^{e+f-n}\xi_{s_{im}}\mu_{s_{im}} + \sum_{i=e+f-n+1}^{m}\frac{T_d - \beta_{m-1}}{\Delta T}\mu_{s_{im}} \qquad (8)$$

from which, the expression for T_d can be obtained as

$$T_d = \beta_{m-1} + \frac{\Delta T}{\sum_{i=e+f-n+1}^{m}\mu_{s_{im}}} \times \left(Y_d - \sum_{j=1}^{m-1}\sum_{i=1}^{j}\mu_{s_{ij}} - \sum_{j=m+1}^{K}\sum_{i=1}^{j}\xi_{s_{ij}}\mu_{s_{ij}} - \sum_{i=1}^{e}\mu_{s_{im}} - \sum_{i=e+1}^{e+f-n}\xi_{s_{im}}\mu_{s_{im}}\right) \qquad (9)$$

By replacing n with the value of $0,\cdots,f$ in turn in the above equation, all the possible solutions (i.e. $T_{d_1}, T_{d_2}, \cdots, T_{d_{f+1}}$) for T_d can be calculated and the exact value of T_d is determined as the minimum, namely

$$T_d = H^{-1}(Y_d) = \min\left\langle T_{d_1}, T_{d_2}, \cdots, T_{d_{f+1}} \right\rangle \qquad (10)$$

When the desired output is decreasing, the similar deduction procedure is carried out. For the target output $Y_d < Y_c$, the required input should be $T_d < T_c$. Then the MKP operators will be evolved along the negative α axis. By starting the direct calculation of the forward MKP hysteresis model from $T = \alpha_p$ in decrement of ΔT until $H(\alpha_{m-1}) \le Y_d$, it can be determined that $T_d \in [\alpha_{m-1}, \alpha_m)$. In this case, the final link of the interface to be created is a vertical one and locates on the column m. Suppose on the column m, there are

$e+1$ operators with the previous output states of +1, which correspond to the grid points $s_{mm} \sim s_{m,m+e}$, f operators with the intermediate output states previously, which correspond to the grid points $s_{m,m+e+1} \sim s_{m,m+e+f}$, and the rest with the previous output states of 0, which correspond to the grid points $s_{m,m+e+f+1} \sim s_{mK}$. Similar arguments as for $Y_d > Y_c$ can reveal that there are $f+1$ possible solutions for T_d. According to the expression for Y_d, i.e.

$$Y_d = \sum_{i=1}^{m-1}\sum_{j=i}^{K} \xi_{s_{ij}} \mu_{s_{ij}} + \sum_{j=m}^{m+e+n} \frac{T_d - \alpha_{m-1}}{\Delta T} \cdot \mu_{s_{mj}} + \sum_{j=m+e+n+1}^{m+e+f} \xi_{s_{mj}} \mu_{s_{mj}} \tag{11}$$

The formula for T_d in the case of decreasing output can be obtained as

$$T_d = \alpha_{m-1} + \frac{\Delta T}{\sum_{j=m}^{m+e+n} \mu_{s_{mj}}} \cdot (Y_d - \sum_{i=1}^{m-1}\sum_{j=i}^{K} \xi_{s_{ij}} \mu_{s_{ij}} - \sum_{j=m+e+n+1}^{m+e+f} \xi_{s_{mj}} \mu_{s_{mj}}) \tag{12}$$

where n denotes the number of the operators on the column m that are switched from the intermediate output states to the new lower ones. By replacing n with the value of $0,1,\cdots,f$ in turn in the above equation, all the possible solutions (i.e. $T_{d_1}, T_{d_2}, \cdots, T_{d_{f+1}}$) for T_d can be calculated and the exact value of T_d is determined as the maximum one of them, namely

$$T_d = H^{-1}(Y_d) = \max\left\langle T_{d_1}, T_{d_2}, \cdots, T_{d_{f-e+1}} \right\rangle \tag{13}$$

In the case of the target output is the same as the current one, i.e. $Y_d = Y_c$, the target input keeps the same value of the current input, i.e.

$$T_d = H^{-1}(Y_d) = H^{-1}(Y_c) = T_c \tag{14}$$

Using the equations (8)~(14) for the inverse MKP model, the input required for the hysteresis system to achieve a desired output can be predicted.

5. Numerical simulations

So far, the MKP model and its inverse model have been completely presented. Following that, they were applied to simulate the actual response of an SMA hysteresis plant, in order to evaluate their performances.

5.1 Matlab/Simulink programme

Based on the numerical formulas derived in the previous sections, the MKP hysteresis model and the inverse MKP hysteresis model were programmed as several functions in the computer language C, and then transferred to the S-functions compatible with Matlab/ Simulink by the use of its S-Function Builder. Referring to the corresponding S functions, two user-defined Simulink blocks, respectively named as sf_MKP and sf_Inverse_MKP were built to implement the MKP hysteresis model and the inverse MKP hysteresis model respectively in this software environment. The different simulation tasks were realized by

using these blocks and the convenient post-processing was also available to display the results graphically.

5.2 Data preparation

Experimental work were carried out on a simple SMA hysteresis plant at room temperature, which was a commercial NiTi tension spring (Mondo-Tronics Inc., Canada) under a dead mass of 6N. The specifications of this NiTi tension spring is shown in Table 1. In the experiment, it experienced one complete actuation cycle and a number of partial actuation cycles by alternately passing an electric current of 2A to heat it and switching off the current to cool it. Its temperature and the corresponding displacement during this experimental process were measured by the use of a thermocouple and a LVDT respectively, and stored in the matrix format of $T = [\text{TimeValues DataValues}]$ and $Y = [\text{TimeValues DataValues}]$. Such an experiment was repeated twice. Then two sets of data involving both major loop and minor loops (i.e. multiple loops) of this hysteresis plant were acquired. Prior to the simulation tests, they were filtered to remove the noise and disturbance.

Table 1. Specifications of the NiTi tension spring

Wire diameter (mm)	0.75
Coil diameter (mm)	6
Length (mm)	30
Nominal actuation temperature range upon heating (°C)	45 ~ 65

The discrete Preisach plane for the MKP model and the inverse MKP model was defined with the specific values of the related parameters as given in Table 2. Then the parameters of the models (i.e. the weighting values for the MKP operators) were identified by means of the simple least-squares fitting of one set of measured data, which was represented by $\hat{\mu}$. Fig.8 (a, b) illustrates the weighting values in the Preisach plane and in 3D curves respectively. According to the distribution of non-zero weighting values, it can be estimated that the actuation temperature ranges of the NiTi tension spring are about 30°C ~80°C upon heating and 25°C ~50°C upon cooling respectively. The other set of measured data were adopted as the input signal to the MKP model and inverse MKP model in the simulation tests.

Table 2. Definition of the discrete Preisach plane for MKP model and inverse MKP model

Discretization level	$K = 20$
Number of MKP operators	$N = \frac{K \times (K+1)}{2} = 210$
Input temperature range (°C)	$T \in [20,80]$
Nominal actuation temperature range Interval (°C)	$\Delta T = [80-20]/(K-1) = 3.16$

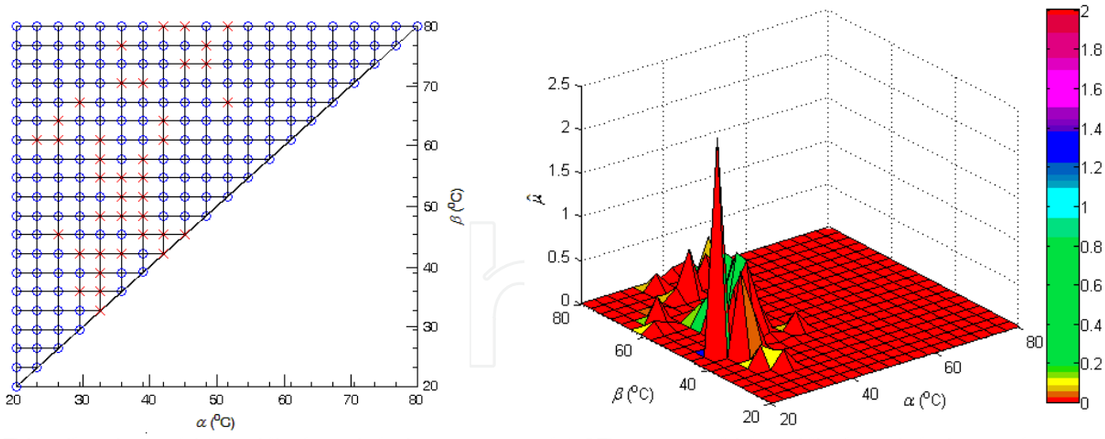

(a) Distribution of identified weighting values in Preisach plane (o: zero weighting value; ×: non-zero weighting value)

(b) 3D curve of identified weighting values

Fig. 8. Identified weighting values

5.3 Simulation tests

Two types of simulation tests were conducted here. One was the use of the MKP model to simulate the output of the NiTi tension spring in response to the measured temperature, while the other, on the contrary, was the use of inverse MKP model to predict the temperature, given the measured displacement. The graphical diagrams for these simulation tests by Matlab/Simulink are shown in Fig. 9.

(a) Simulation test on MKP model

(b) Simulation test on inverse MKP model

Fig. 9. Matlab/Simulink diagram for the simulation tests

6. Results

6.1 Results of the simulation test on MKP model

Fig.10 illustrates the results of the simulation test on MKP model in terms of the modelled displacement vs. time curve, which is compared with the measured one. It is clear that the modelled displacement matches the measured one to a great extent.

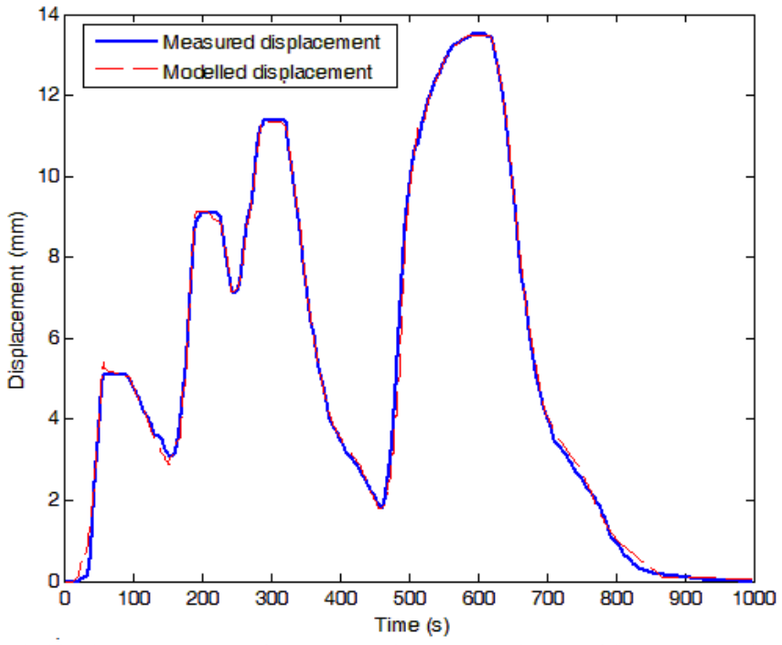

Fig. 10. Modelled displacement vs. time curve in comparison with measured one

The slight difference is mainly observed in the segments associated with the transition between a rising branch and a falling branch of the displacement curve. This phenomenon is more clearly demonstrated in the input temperature vs. output displacement curves as shown in Fig.11. The modelled multiple loops have a great resemblance to the measured one. To give a further quantitative analysis, the discrepancy between the modelled displacement and the measured one is calculated and plotted in Fig.12. Apparently, it is up to the bound of ±0.5mm, which is actually quite small.

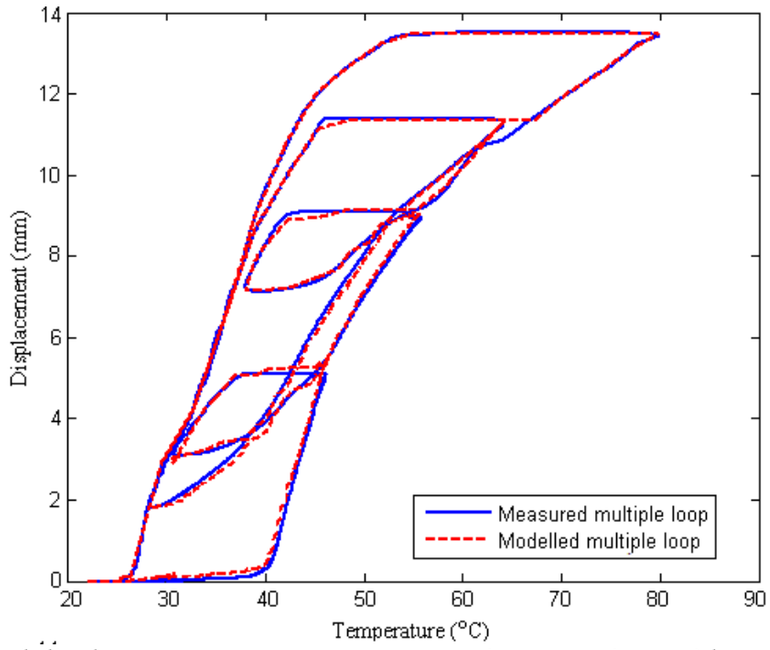

Fig. 11. Modelled displacement vs. temperature curve in comparison with measured one

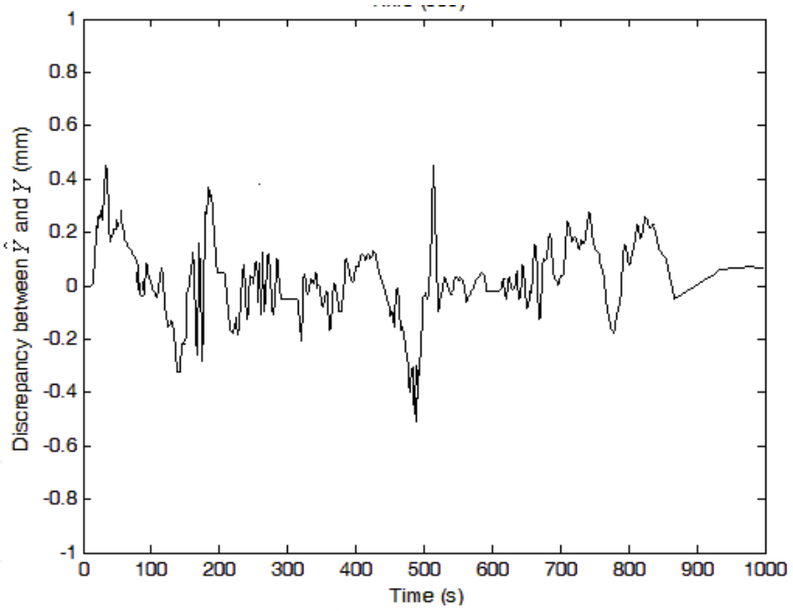

Fig. 12. Discrepancy between modelled displacement and measured one

6.2 Results of the simulation test on inverse MKP model

The temperature calculated from the inverse MKP model (i.e. the modelled temperature) in response to the measured displacement is shown in Fig.13 as a function of time. For comparison purpose, the measured temperature vs. time curve is also plotted here. It can be seen from the figure that the modelled temperature is very close to the measured one for the most of time. Exceptionally, when the measured temperature starts to rise or fall each time, the modelled temperature fails to follow it immediately. There seems to be a lag initially in

each ascending or descending branch of the modelled temperature curve behind the measured one. The time history of the discrepancy between them is presented in Fig.14 , which reveals this phenomenon more clearly.

Actually, this phenomenon is resulted from the hystersis behaviour of SMA. Referring to the measured temperature vs. displacement curve (marked in bold line, Fig.11), each time when the measured temperature alternates the change direction, the measured displacement does not change with the measured temperature immediately. Instead, it keeps constant for some time while the measured temperature rises or falls. Moreover, recalling to the previous deduction process(see section 4), the inverse MKP model is actually deduced in such a way that its output (i.e. modelled temperature) changes when the input displacement changes, while keeps the value in response to the previous displacement, when the subsequent displacement is the same as the previous one. Take the fourth descending branch of the modelled temperature curve for example. To be able to view the details, close-up view of the modelled temperature, measured temperature and measured displacement curves from 550s to 700s is illustrated in Fig.15. Apparently, during the period of 586s~622s when the measured displacement, as the input to the inverse MKP model, is almost constant at about 13.5mm, the modelled temperature stays at a constant value of about 79°C, while the measured temperature keeps falling from 79°C to 53°C. As a result, the discrepancy between them increases rapidly and reaches the maximum value 26°C at the time instant of 622s (see Fig.14). Then at the next time instant (i.e. 623s), as the measured displacement starts to decrease, the modelled temperature drops to about 51°C and gradually catch the measured one since then. The discrepancy between them is less than 2°C, following the further deceasing measured displacement.

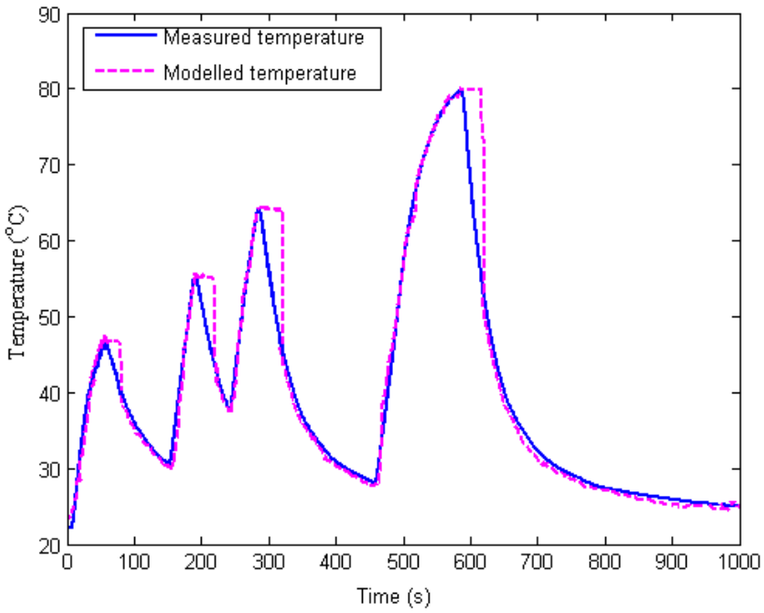

Fig. 13. Modelled temperature vs. time curve in comparison with measured one

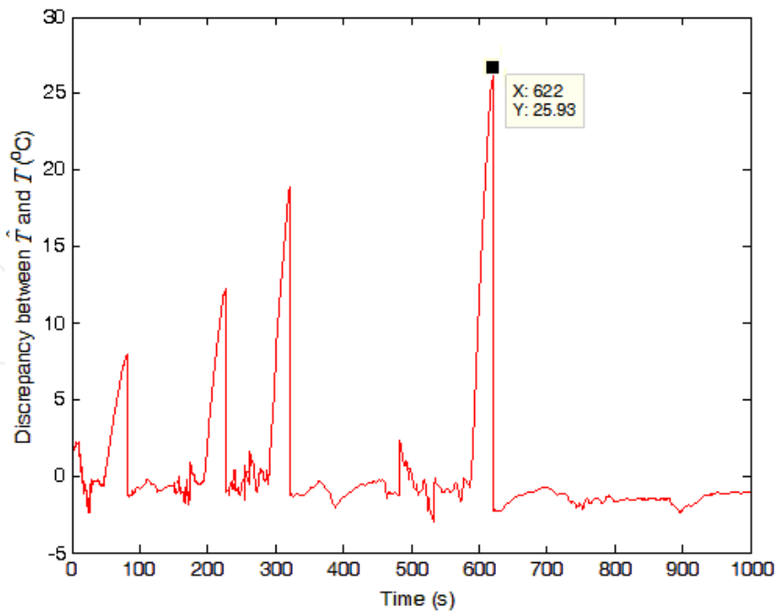

Fig. 14. Discrepancy between modelled temperature and measured one

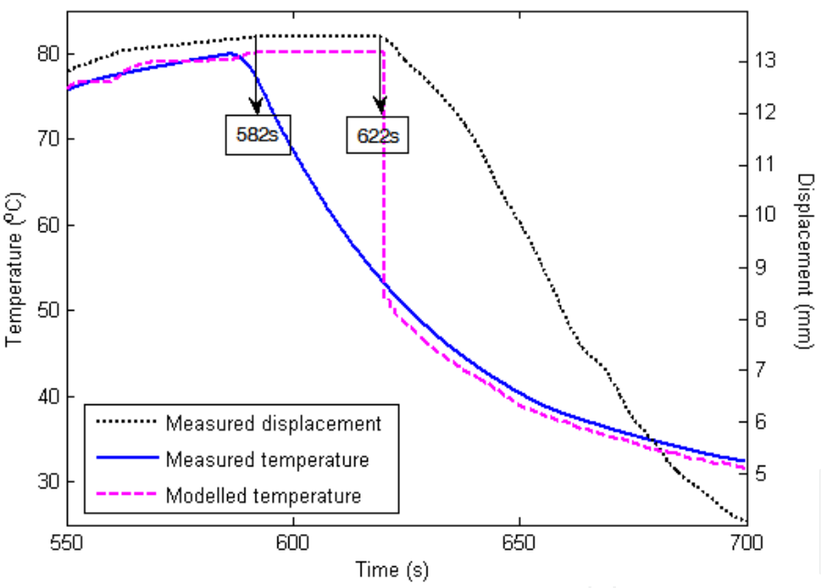

Fig. 15. Close-up view of measured displacement, measured temperature and modelled

7. Discussion

In the laboratory situation, there are always some degrees of measurement error in the data acquired mainly due to the accuracy of the sensors used in measuring the temperature of SMA actuators, e.g. thermocouple, and in measuring their displacement, e.g. LVDT. The accuracy specification for thermocouple and that for LVDT used here are ±1 °C and ±0.5 mm (i.e. ±1% of its measurement range of 50mm). Meanwhile, the weighting values identified by means of the least-square fitting are not the exact ones. These factors mainly

account for the small discrepancy between the modelled displacement and the measured displacement, and the one between the modelled temperature and the measured temperature when the measured displacement changes.

It is also important to point out that the accuracy of MKP model and inverse MKP model strongly depends on the parameter identification. These characteristic parameters of the models are directly connected with the macroscopic experimental facts. Typically, they are determined by means of simple interpolation of the limited experimental data or least-squares fitting of a measured major loop or multiple loops for a pre-selected load (Torrie & Vajida, 1994; Song et al, 2001; Ktena et al, 2001). Such identification strategies are strongly sensitive to measurement errors. More seriously, the hysteresis behaviour of SMA actuators varies with the applied stress, pre-deformation (see Fig. 2) and the number of thermal/ mechanical cycles. Therefore, such an off-line identified hysteresis model as an input-output static mapping cannot accommodate the dynamic changes and even introduces input error, when it is ill-matched to the real response of the hysteretic system. For example, if the loading condition of the NiTi tension spring were changed from 6N to 10N, the MKP model identified for it under a load of 6N here could not portray its hysteresis behaviour under a load of 10N. In the real control applications, SMA hysteresis plant is often associated with significant uncertainties such as the various loading conditions. Obviously, the off-line identified MKP model and inverse MKP model is unable to capture the real hysteris response. Instead, on-line update of the parameters should be incorporated in the control scheme based on MKP model and inverse MKP model, in order to achieve the accurate control.

8. Conclusions

MKP model proposed in this study is independent of the specific plant and thus is generally applicable to different hysteretic systems incorporating SMA actuators. The condition is that Preisach plane must be defined to cover the actuation temperature range of SMA actuators in use, which is rather weak and can be easily satisfied. Its advantage in the reduced computation is obvious and makes it more suitable for control purpose. The accuracy of MKP and inverse MKP models strongly depends on parameter identification. The results of the numerical simulation have successfully demonstrated that MKP and inverse MKP models are able to model and predict the response of SMA hysteresis plants, when their parameters identified by the use of the limited experimental data are sufficiently accurate. Since the off-line identified models cannot accomodate the unmodelled dynamics, it is necessary to correct them on-line to achieve hysteresis compensation for SMA hysteresic system with unknown dynamics such as various loading conditions in the real control applications. Noticeably, the expression of MKP model in the linearly parameterized form allows the general adaptive method, such as the gradient estimator, to be a handy choice for on-line parameter update. The findings are encouraging for moving to the development of control schemes based on MKP and inverse MKP models.

9. References

Bhattacharyya, A. & Lagoudas, D. (1997). Smart Materials &Structures, 6, 3, 235-250

De Sars, V.; Haliyo, S. & Szewczyk, J. (2010). Mechatronics, 20, 2, 251-264

Dickson Carrie, A.; Hughes Declan, C. & Wen John, T. (1996). Hysteresis in shape memory alloy actuators: the control issues, Proceedings of SPIE, 2715, 494-506

Gupta, K.; Darpe, A.; Kumar. B.; et al. (2009). Advances in Vibration Engineering, 8, 3, 247-254

Hughes, D. & Wen, J. (1997). Smart Materials & Structures, 6, 287-300

Krasonselskii, M. & Pokrovskii, A. (1989). Systems with Hysteresis, Springer-Verlag, Heidelberg

Krasonselskii, M.; Pokrovskii, A.; Rachinskii, D.; et al. (1994). Automation and Remote Control, 55, 7, 964-973

Ktena, A.; Fotiadis, D. ; Spanos, P.; et al. (2001). Physica B, 306, 84-90

Matsuzaki, Y. & Naito, H. (2004). Journal of Intelligent Material Systems and Structures, 15, 2, 141:155

Mayergoyz, I. (1991). Mathematical models of hysteresis, Springer-Verlag, Berlin

Okamura, H.; Yamaguchi, K. & Ono, R. (2009). International Journal of Optomechatronics, 3, 4, 277-288, 1559-9612

Popov, P. & Lagoudas, D. (2007). International Journal of Plasticity, 23, 4, 1679-1720.

Ŝittner, P.; Stalmans, R. & Tokuda, M. (2000). Smart Materials & Structures, 9, 452-465

Song, C.; Brandon, J. & Featherston C. (2001). Distributed-element Preisach model for hysteresis of shape memory alloys, Proc Instn Mech Engrs, 215 (part C), 673-682

Torrie, E. & and Vajda, F. (1994). IEEE Transactions on Magnetics, 30, 6, 4987-5000

Van Humbeeck, J. & Stalmans, R. (1998). Characteristics of shape memory alloys, In: Shape Memory Materials, Otsuka, K. &Wayman, C. (Ed.), 149-184, Cambridge University Press, Cambridge

Wang, J. & Dai, H. (2010). International Journal of Plasticity, 26, 4, 467-487

Wayman, C. & Duerig, T. (1990). An Introduction to martensite and shape memory, In: Engineering Aspects of Shape Memory Alloys, Duerig, T. (Ed.), 3-20, Butterworth – Heinemann Ltd., London

Webb, G. & Lagoudas, D. (1998). Journal of Intelligent Materials and Structures, 9, 432- 448

Wolfe, T.; FaulKner, M. & Wolfaardt, J. (2005). Smart Materials & Structures, 14, 4, 759-768, 0964-1726

Wong, F.; Rabbath, C.; Hamel, N.; et al. (2007). Transactions of the Canadian Society for Mechanical Engineering, 31, 1, 19-38

IntechOpen

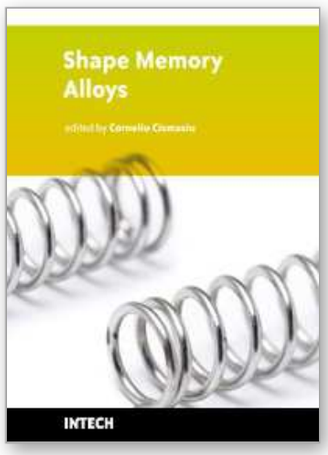

Shape Memory Alloys

Edited by Corneliu Cismasiu

ISBN 978-953-307-106-0
Hard cover, 210 pages
Publisher Sciyo
Published online 18, October, 2010
Published in print edition October, 2010

In the last decades, the Shape Memory Alloys, with their peculiar thermo-mechanical properties, high corrosion and extraordinary fatigue resistance, have become more popular in research and engineering applications. This book contains a number of relevant international contributions related to their properties, constitutive models and numerical simulation, medical and civil engineering applications, as well as aspects related to their processing.

How to reference

In order to correctly reference this scholarly work, feel free to copy and paste the following:

Hongyan Luo, Yanjian Liao, Eric Abel, Zhigang Wang and Xia Liu (2010). Hysteresis Behaviour and Modeling of SMA Actuators, Shape Memory Alloys, Corneliu Cismasiu (Ed.), ISBN: 978-953-307-106-0, InTech, Available from: http://www.intechopen.com/books/shape-memory-alloys/hysteresis-behaviour-and-modeling-of-sma-actuators-

INTECH
open science | open minds

InTech Europe
University Campus STeP Ri
Slavka Krautzeka 83/A
51000 Rijeka, Croatia
Phone: +385 (51) 770 447
Fax: +385 (51) 686 166
www.intechopen.com

InTech China
Unit 405, Office Block, Hotel Equatorial Shanghai
No.65, Yan An Road (West), Shanghai, 200040, China
中国上海市延安西路65号上海国际贵都大饭店办公楼405单元
Phone: +86-21-62489820
Fax: +86-21-62489821

IntechOpen